Structural and Dynamic Characterization of ω-Conotoxin MVIIA: The Binding Loop Exhibits Slow Conformational Exchange[†,‡]

R. Andrew Atkinson,*[,§] Bruno Kieffer, Annick Dejaegere, Finton Sirockin, and Jean-François Lefèvre

UPR 9003 du CNRS, Ecole Supérieure de Biotechnologie de Strasbourg, Bld. Sébastien Brant, 67400 Illkirch, France

Received November 16, 1999; Revised Manuscript Received January 20, 2000

ABSTRACT: ω-Conotoxin MVIIA is a 25-residue, disulfide-bridged polypeptide from the venom of the sea snail *Conus magus* that binds to neuronal N-type calcium channels. It forms a compact folded structure, presenting a loop between Cys8 and Cys15 that contains a set of residues critical for its binding. The loop does not have a unique defined structure, nor is it intrinsically flexible. Broadening of a subset of resonances in the NMR spectrum at low temperature, anomalous temperature dependence of the chemical shifts of some resonances, and exchange contributions to $J(0)$ from ^{13}C relaxation measurements reveal that conformational exchange affects the residues in this loop. The effects of this exchange on the calculated structure of ω-conotoxin MVIIA are discussed. The exchange appears to be associated with a change in the conformation of the disulfide bridge Cys8-Cys20. The implications for the use of the ω-conotoxins as a scaffold for carrying other functions is discussed.

Sea snails of the genus *Conus* use venom containing a battery of molecules for hunting. Each species of sea snail produces a distinct set of toxins adapted to its particular food source (*1*). The components of these toxins are targeted to specific receptors in the sea snail's prey. These molecules, termed conotoxins, are also subtype-specific ligands for analogous receptors in mammals (*2*). Thus, for example, α-conotoxins bind specifically to nicotinic acetylcholine receptors and ω-conotoxins to neuronal N-type calcium channels (*3*). Each of these ligands may serve as a pharmacological tool—indeed, ω-conotoxin binding is widely used in defining calcium channel types—and as a template for drug design (*4*).

Many of the conotoxins are short peptides (9−35 amino acids) and contain a high proportion of cysteine residues, forming distinctive sets of disulfide bridges. The pattern of cross-links is often conserved among the conotoxins of different species that bind to the same class of receptors. The structures of several ω-conotoxins have been determined, each describing a small, triple-stranded β-sheet, tightly cross-linked by three disulfide bridges (*5*−*11*). The same topology was identified in a number of other polypeptides with diverse functions (*12*). The toxins from different species of sea snail show great variety, however, in the nature of the side chains at other positions, even when exhibiting similar binding properties: both ω-conotoxins GVIA and MVIIA, for example, bind to neuronal N-type calcium channels, but ω-conotoxin GVIA is rich in hydroxyl groups, while ω-conotoxin MVIIA contains a large number of positively charged side chains. Chemical modification and peptide synthesis have identified a number of key residues for binding, including several located in the central loop between the second and third cysteine residues (*13*−*15*). In particular, it has been shown that the hydroxyl group of the tyrosine residue at position 13 is essential for the activity of ω-conotoxins (*16*) and that, while residues 9−14 all play a role in binding to calcium channels, Leu11 and Tyr13[1] are the most important residues (*17, 18*).

Initial reports of the determination of the structure of ω-conotoxin MVIIA (*8,9*) suggested that its binding loop exhibited greater flexibility than the cross-linked core of the molecule. Nielsen et al. (*11*) noted, however, that broadening of residues 11−13 indicated the presence of conformational exchange in this key loop. This phenomenon is explored in detail here through the effects of temperature variation, ^{13}C relaxation at natural abundance, structure determination, and chemical shift calculations. The possible origins and consequences of conformational exchange in ω-conotoxin MVIIA are discussed as are its implications for understanding conotoxin binding.

EXPERIMENTAL PROCEDURES

Sample Preparation. A lyophilized sample of 10 mg of ω-conotoxin MVIIA was dissolved in 600 μL of H_2O (10% D_2O) to give a final concentration of 6.3 mM. Small aliquots

[†] R.A.A. gratefully thanks Eli Lilly for the award of a postdoctoral fellowship as part of the CNRS-ULP-E.Lilly research agreement.

[‡] Coordinates of ω-conotoxin MVIIA determined with and without χ_3 constraints on disulfide bridges have been deposited at the Protein Data Bank under accession numbers 1DW4 and 1DW5, respectively.

[§] Present address: National Institute for Medical Research, The Ridgeway, Mill Hill, London NW7 1AA, U.K.

* Address correspondence to this author at the National Institute for Medical Research, The Ridgeway, Mill Hill, London NW7 1AA, U.K. Tel: (+44) (0)208 959 3666. Fax (+44) (0)208 906 4477. E-mail: aatkins@nimr.mrc.ac.uk.

[1] Abbreviations: COSY, 2D correlated spectroscopy; CPMG: Carr−Purcell−Meiboom−Gill; HOHAHA, 2D homonuclear Hartmann−Hahn spectroscopy; HSQC, heteronuclear single quantum coherence spectroscopy; NOE, nuclear Overhauser enhancement; NOESY, 2D NOE spectroscopy; TPPI, time-proportional phase incrementation. Standard one- and three-letter abbreviations are used for the amino acids throughout.

10.1021/bi992651h CCC: $19.00
Published on Web 03/18/2000

of HCl were used to adjust the pH to 3.5 (direct meter reading). For hydrogen exchange measurements, diffusion, and ^{13}C relaxation experiments, the sample was lyophilized and dissolved in D_2O. A small amount of DSS (sodium 2,2-dimethylsilapentane 5-sulfonate) was used as an internal reference.

^1H NMR Measurements. All NMR measurements were carried out at 283 K (unless stated otherwise) and at 500 or 600 MHz on Bruker AMX500 or DRX600 spectrometers.

Standard two-dimensional ^1H experiments were carried out at 600 MHz in phase-sensitive mode, using either the method of States et al. (*19*) or time-proportional phase incrementation (TPPI, *20*), with a spectral width of 7003 Hz in both dimensions and a relaxation delay of 3 s. COSY (*21*) and HOHAHA (*22*,*23*) spectra were recorded with presaturation of the water signal during the relaxation delay, and, for the HOHAHA experiment, with a spin-locking rf field strength of ca. 8.5 kHz and mixing times of 40 and 80 ms. NOESY (*24*) spectra were recorded with suppression of the water signal using a WATERGATE sequence (*25*,*26*) prior to acquisition and with mixing times of 50, 100, 150, 200, 250, and 300 ms. In most cases, 32 transients of 2K data points were acquired per t_1 increment, with 512 t_1 increments for experiments using TPPI and 256 increments for those using the method of States et al. (*19*).

Spectra were processed using the manufacturer's software, UXNMR, and using Felix (v2.1, Biosym Technologies, San Diego, CA). COSY data was multiplied by an unshifted sine bell and HOHAHA and NOESY data by a 90°-shifted sine bell prior to zero-filling once and Fourier transformation.

Hydrogen Exchange. Hydrogen−deuterium exchange was investigated by recording a series of one-dimensional ^1H spectra and NOESY spectra (as above, except that only 256 t_1 increments were acquired) at 600 MHz, immediately following dissolution in D_2O and over the subsequent 24 h. Intensities of amide HN peaks in 1D spectra were measured, scaled to the intensity of the peaks of the single aromatic residue, Tyr13, and fitted with a single exponential in Matlab (The MathWorks Inc., Natick, MA) by simplex minimization and Levenberg−Marquardt nonlinear regression to give values of k_{ex}. The fit was checked visually and by verifying the linearity in a log plot of the signal intensity versus time.

Temperature Studies. One-dimensional ^1H spectra were recorded at 1° intervals between 275 and 304 K, at 600 MHz. At 275 K, HOHAHA spectra with mixing times of 40 and 80 ms were recorded, and NOESY spectra with a mixing time of 150 ms were recorded at 5° intervals between 275 and 304 K, all as described above, except that only eight transients were acquired per increment and, for the NOESY spectra, only 384 t_1 increments were made. The slopes of the plots of the chemical shifts of the amide HN resonances versus temperature were determined by linear regression using Matlab.

^{13}C NMR Measurements. ^{13}C-^1H HSQC spectra (*27*) were acquired at 600 MHz (^1H frequency) and at 275 and 283 K, using the sample of unlabeled ω-conotoxin MVIIA in H_2O (10% D_2O). The water signal was suppressed by irradiation during the relaxation delay (3 s). The pulse sequence employed echo-antiecho gradient selection to achieve sensitivity enhancement (*28*), and ^{13}C nuclei were decoupled during acquisition by a GARP sequence (*29*). A total of 512 t_1 increments were acquired with 32 transients of 2K data points per increment. Spectral widths of 7003 and 20 000 Hz were set for t_2 (^1H) and t_1 (^{13}C), respectively.

A full set of ^{13}C relaxation measurements (T_1, T_2, and heteronuclear NOE) were carried out at both 500 and 600 MHz (^1H frequency) using the sample of unlabeled ω-conotoxin MVIIA transferred into D_2O. Experiments used to measure the rates of longitudinal and transverse relaxation ($R_C(C_z)$ and $R_C(C_{x,y})$) and the heteronuclear NOE (R_C ($H_z \rightarrow C_z$)) for $^{13}C\alpha$ and threonine $^{13}C\beta$ nuclei were based on those described by Dayie and Wagner (*30*). All pulse sequences employed ^1H detection, sensitivity enhancement by echo-antiecho gradient selection, and ^{13}C decoupling during acquisition using a GARP sequence. For all experiments, the residual water signal was suppressed by irradiation during the relaxation delay (3−3.5 s), and 2K data points were acquired in t_2. At 600 MHz, the spectral widths were set to 6009 and 6000 Hz for t_2 (^1H) and t_1 (^{13}C), respectively, while at 500 MHz, the spectral width was set to 5000 Hz in both dimensions. A total of 48 or 64 transients were acquired for each of 256 t_1 increments for $R_C(C_z)$ and $R_C(C_{x,y})$ measurements; only 128 t_1 increments were made for the heteronuclear NOE measurements.

In $R_C(C_z)$ experiments at 600 MHz, the values of the recovery delay were 0.001, 0.01, 0.02, 0.05, 0.1 (2×), 0.2, 0.3, 0.4, 0.5, 0.6, 0.7, 0.8, 1.0, and 1.5 s, while at 500 MHz, the delays were: 0.001, 0.002, 0.005, 0.01, 0.02, 0.04, 0.06, 0.08, 0.12, 0.2, 0.4, 0.5, 0.75, and 1.0 s. In $R_C(C_{x,y})$ experiments at 600 MHz, the total delays for the CPMG sequence (with 0.4 ms between pulses) were 2.7, 16.4 (2×), 32.8, 41.0, 49.2, 57.5, 65.7, 98.5 (2×), 114.9, 131.3, 147.7, 164.2, 180.6 and 197.0 ms, while at 500 MHz the total delays were: 1.6, 4.4, 9.9, 18.2 (2×), 26.4, 34.7, 51.3, 67.8, 101.0, 134.1, and 167.2 ms. In the heteronuclear NOE experiments, the ^1H nuclei were irradiated (or not) during 6.5 s, using a series of 40 μs pulses at 5 ms intervals.

Analysis of Relaxation Data. The intensities of cross-peaks in the series of $R_C(C_z)$, $R_C(C_{x,y})$, and heteronuclear NOE measurements were extracted. Curves for $R_C(C_z)$ and $R_C(C_{x,y})$ were fitted in Matlab, using a single exponential, by simplex minimization and Levenberg−Marquardt nonlinear regression to give values of $R_C(C_z)$ and $R_C(C_{x,y})$. The fit was checked visually and by verifying the linearity of the plot of the log of the intensity versus time. Values of $R_C(H_z \rightarrow C_z)$ were calculated from the intensities of the experiments recorded with and without saturation of the ^1H nuclei, using the values of $R_C(C_z)$

$$R_C(H_z \rightarrow C_z) = \left(\frac{\gamma_C}{\gamma_H}\right)\eta R_C(C_z) \qquad (1)$$

where

$$\eta = \left(\frac{I_{sat}}{I_{unsat} - 1}\right)$$

In the reduced spectral density function approach (*31*−*36*), the relaxation rates are expressed in terms of the spectral density, $J(\omega)$, at frequecies 0, ω_C and $\langle\omega_H\rangle$.

$$\begin{pmatrix} R_C(C_z) \\ R_C(C_x) \\ R_C(H_z \rightarrow C_z) \end{pmatrix} = \begin{pmatrix} 0 & E & 7A \\ 2E/3 & E/2 & 13A/2 \\ 0 & 0 & 5A \end{pmatrix} \begin{pmatrix} J(0) \\ J(\omega_C) \\ \langle J(\omega_H)\rangle \end{pmatrix}$$

or

$$\mathbf{R} = \mathbf{C} \times \mathbf{J} \tag{2}$$

where

$$A = \left(\frac{\mu_0}{4\pi}\right)^2 \frac{\gamma_H^2 \gamma_C^2 h^2}{4r_{CH}^6}$$

$$E = 3A + B$$

and

$$B = \Delta_C^2 \omega_C^2/3$$

where μ_0 is the permeability of the vacuum, γ_H and γ_C are the gyromagnetic ratios of the ^{1}H and ^{13}C nuclei, respectively, r_{CH} is the internuclear ^{13}C−^{1}H bond distance (r_{CH} = 1.07 Å), and Δ_C is the chemical shift anisotropy of ^{13}C ($\Delta_C\alpha$ = 25 ppm, *37*).

The values of the spectral density, $J(\omega)$, at frequencies 0, ω_C, and $\langle\omega_H\rangle$ may thus be obtained simply by inverting eq 2:

$$\mathbf{J} = \mathbf{C}^{-1} \times \mathbf{R} \tag{3}$$

This approach assumes that the spectral density is the same between $\omega_H - \omega_X$ and $\omega_H + \omega_X$. While this has been shown to introduce little error for ^{15}N measurements (*34*), where $\langle J(\omega_H)\rangle \approx J(\omega_H + \omega_X)$, it introduces considerable error for ^{13}C data (*38*). The spectral density around ω_H was therefore also modeled as a single Lorentzian, characterized by a time, τ_H. The measured relaxation rates were fitted using three parameters, $J(0)$, $J(\omega_C)$, and τ_H. The values of $J(\omega_H - \omega_C)$, $J(\omega_H)$, and $J(\omega_H + \omega_C)$ were recalculated using the trial value of τ_H using

$$J(\omega) = \frac{2}{5}\frac{\tau_H}{1 + \omega^2\tau_H^2} \tag{4}$$

and the trial values of the relaxation rates, $R_C(C_z)$, $R_C(C_{x,y})$, and $R_C(H_z \rightarrow C_z)$, were calculated as in eq 2. Here, a simulated annealing algorithm, as described by Kirkpatrick et al. (*39*) and implemented by Goffe et al. (*40*), was used, although any other minimization protocol might be used.

Modules of the suite of programs Relaxmax (J.-F. Lefèvre, unpublished) were used to analyze the spectral density values and extract the correlation times for overall motion and rapid internal motion.

Diffusion Measurements. The translational diffusion constant of ω-conotoxin MVIIA was measured in D_2O at 298 K by observing the decay of double quantum coherences using a gradient-stimulated spin−echo sequence (*41*−*43*). This procedure allows a scale-up of the gradient effects by a factor of 4 and thus increases the precision of the diffusion coefficient measurement. A modification of the double quantum spin−echo sequence (*43*) was used here, in which the total length of the echo ($2\tau + 4\delta$) is kept constant:

$$d1 - S_1 - \delta(g_Z) - (\tau - t_1) - \delta(G_Z) - t_1 - P_{180} - t_1 - \delta(G_Z) - (\tau - t_1) - \delta(g_Z) - S_2 - \text{acq}$$

The sequence $S_1 = P_{90} - \epsilon - P_{180} - \epsilon - P_{90}$ is used to produce double quantum coherence and $S_2 = P_{90} - \epsilon - P_{180} - (\epsilon - \delta) - \delta(2g_z)$ converts double quantum coherences back into in-phase observable magnetization. The intensities of the peak heights measured at increasing values of the delay t_1 could be fitted to the following expression (*44*)

$$M(t_1) = M_o \exp\left(-(2\gamma_H G_Z s\delta)^2 D_t\left(\Delta - \frac{\delta}{3}\right)\right) \tag{5}$$

where $\Delta = \delta + P_{180} + 2t_1$, M_o is the magnetization at t_1 = 0, γ_H is the gyromagnetic ratio of ^{1}H, D_t is the translational diffusion coefficient, s is a gradient shape factor, G_Z is the Z-gradient intensity, and δ is the gradient length.

Measured diffusion coefficients were corrected to standard conditions (H_2O at 293 K) using a viscosity ratio of 1.23 between H_2O and D_2O. A total of 64 experiments were recorded with a t_1 increment of 1 ms and with the following parameters: G_Z = 28 G cm^{-1}, g_Z = 7 G cm^{-1}, δ = 3 ms, τ = 65 ms and ϵ = 10 ms. The gradient strengths were calibrated by imaging a hole of known length in a Teflon phantom and by measuring the diffusion of the residual water using a single quantum gradient-stimulated echo sequence.

Structural Constraints. The intensities of cross-peaks in the NOESY spectrum recorded with a mixing time of 50 ms were measured. An initial calibration based on the intensity of vicinal protons was relaxed such that the distances corresponding to HN_i−HN_{i+1}, HN_i−$H\alpha_i$, and $H\alpha_i$−HN_{i+1} cross-peaks satisfied the expected ranges. This spectrum was estimated to contain data between pairs of protons up to 4.0 Å apart. Intensities were divided into five subsets corresponding to upper distance limits of 2.7, 3.0, 3.3, 3.7, and 4.0 Å. Cross-peaks from the NOESY spectrum recorded with a mixing time of 100 ms were added, using the ratio of intensities of HN_i −HN_{i+1} cross-peaks to scale the intensities to the 50 ms NOESY spectrum. Data between pairs of protons up to 4.7 Å apart could thus be included.

A total of 381 distance constraints, derived from 50 and 100 ms NOESY spectra, were used as upper limits on interproton distances, with no lower limit specified, and applying standard pseudoatom corrections where required (*45*). Of these constraints, 197 were intraresidue, 95 sequential, 30 short range (i.e., (i,j) where $j \leq i + 4$), and 59 long range. Where NOEs to both resonances of unresolved prochiral pairs were observed, both constraints were set to the longer distance with no correction. Disulfide bridges were defined in the topology file with no further constraints.

Coupling constants were measured on cross-sections extracted from a COSY spectrum recorded acquiring 8K data points in t_2. Intensity, line width, phase, and coupling constant were fitted in the time domain, using an in-house program, *fftjval* (P. Koehl, unpublished). Possible values of ϕ angles were calculated from $^3J_{HN-H\alpha}$ values using the Karplus relationship (*46*) and the parameters of Pardi et al. (*47*). Ranges around the calculated value were defined by $^3J_{HN-H\alpha}$ ± 1 Hz. The intensities of HN_i−$H\alpha_i$ NOE cross-peaks were measured to identify positive ϕ angles (*48*).

Intensities of HN−Hβ and Hα−Hβ NOE cross-peaks, together with $^3J_{H\alpha-H\beta}$ values were used to assign prochiral Hβ resonances stereospecifically, where possible (*49*), and to define χ_1 angles. Constraints on these angles were set to the value of the corresponding rotamer ±60° or to exclude one rotamer where data permitted.

Structure Calculations. All calculations were carried out on IBM RS/6000 machines, using standard protocols (dg_sub_embed, dgsa, refine, accept) in X-PLOR 3.1 (*50*), with no modification except as noted. Briefly, substructures are generated using a distance geometry algorithm, then full structures generated and regularized using simulated annealing. Finally, structures are refined, again using a slow-cooling simulated annealing protocol, and structures with poor geometries or large violations of experimental restraints are rejected. Analysis of sets of calculated structures was carried out using in-house X-PLOR scripts and FORTRAN programs. Structures were visualized using Insight (Biosym Technologies, San Diego, CA).

Initial calculations were carried out with no stereospecific assignments and no dihedral angle constraints. Resulting structures were analyzed for consistency with dihedral ϕ and χ_1 angle values and stereospecific assignments derived from spectra and the constraint lists updated. Finally, hydrogen bonds present in more than 80% of calculated structures and for which the HN resonance was observed to exchange slowly into D_2O were added as distance constraints between the HN proton and the acceptor and between the amide nitrogen and the receptor: 1.5 Å < d_{HN-A} < 2.5 Å, 2.5 Å < d_{N-A} < 3.5 Å.

In a further round of calculations, the χ_3 angle across the three disulfide bridges was forced to adopt values around +90° and −90°. To achieve this, the force constant on the dihedral angle $C\beta_i-S\gamma_i-S\gamma_j-C\beta_j$ was set to 40.0 kcal mol^{-1}.

Chemical Shift Calculations. The empirical model developed by Ösapay and Case (*51*) was used to calculate proton chemical shifts. The chemical shift is divided into local diamagnetic and paramagnetic contributions and nonlocal conformation-dependent contributions resulting from the influence of parts of the protein remote in the sequence:

$$\delta_{tot} = \delta_{local} + \delta_{conf} \quad (6)$$

The local contributions are not computed, but are approximated by the observed chemical shifts of short, "random coil" peptides (*52*). The conformation-dependent contribution to the proton chemical shift is estimated by

$$\delta_{conf} = \delta_{tot} - \delta_{randomcoil} = \delta_{rc} + \delta_{ma} + \delta_{el} + \delta_{cst} \quad (7)$$

where "rc", "ma", and "el" refer to ring current, magnetic anisotropy of the peptide group, and electrostatic interactions, respectively. Parameters for these contributions are as defined in the program *shifts* version 3.0b2 (http://www.scripps.edu/case), using the *protein.amber94_nmr* set for the partial charges. The δ_{cst} term is an adjustable parameter that reflects in part the effects of magnetic anisotropy and electrostatics that are present in the "random coil" peptide (*53*).

The program was modified to accept the C-terminal amide group of ω-conotoxin MVIIA. The charges used for this group were −0.908 e$^-$ for N and +0.415 e$^-$ for both H atoms, and it was attributed the same magnetic anisotropy as a peptide bond ($\Delta\chi$ −7.9 erg G^{-2} mol^{-1}). The calculations were performed only for protons directly attached to carbon, since amide proton chemical shifts are influenced by hydrogen bonding and are not well described by the current model (*54*).

RESULTS

Assignment of ^1H and ^{13}C Resonances. All ^1H resonances in the spectrum were assigned in a straightforward manner applying the sequential assignment method, pioneered by Wüthrich (*55*), to a combination of COSY, HOHAHA, and NOESY spectra (see Supporting Information). The assignments were in good agreement with those reported previously (*8*,*9*,*11*) with minor differences for some side chain protons, affected by temperature (vide infra).

^{13}C resonances were assigned to carbon atoms carrying at least one hydrogen atom in the covalent structure (see Supporting Information), from the $^{13}C-^1H$ HSQC spectrum. Only the assignment of some carbon atoms of lysine (Lys2, Lys4, and Lys24) and arginine (Arg10 and Arg21) side chains remained ambiguous.

Hydrogen Exchange. In a NOESY spectrum, recorded 1 h after dissolution of lyophilized ω-conotoxin MVIIA in D_2O, five HN resonances remained. These were assigned to Ala6, Cys8, Gly23, Lys24, and Cys25 (Figure 1) and persisted in a NOESY spectrum recorded 15 h after dissolution. The rate constants for the exchange lie in the range 0.0017 > k_{ex} > 0.0036 min^{-1}, except that of Gly23 which exchanges much more slowly. In the first 1D spectra recorded after dissolution in D_2O, the HN resonances of Gly5, Cys15, and Cys16, and a further resonance at 8.37 ppm (Lys7 or Ser19), were also detected. These protons exchange with rate constants k_{ex} > 0.015 min^{-1}.

Indications of Secondary Structure. The smoothed plot of secondary chemical shifts of Hα resonances (*56*) is negative between Arg10 and Cys15 (suggesting α-helical structure) and positive from Cys16 to the C-terminus (suggesting β-structure), although the effects are not very pronounced (Figure 1). Analysis of the chemical shift indices for the Hα resonances (*57*) identifies only Lys7-Ser9 as a β-strand, while those for the Cα resonances (*58*) are less conclusive. Of course, a lack of elements of regular secondary structure does not imply a lack of defined structure, merely that it may be irregular.

Most striking in the list of distance constraints extracted from NOESY spectra is the wealth of NOEs from Lys24, Cys25, and the C-terminal amide group to protons in the sequence Lys4-Cys8, as well as Cys15 and Cys20. Furthermore, $H\alpha_i-H\alpha_j$ NOEs from Lys24 and Cys25 to Lys7 and Cys20, respectively, indicate that the C-terminus forms a tiny β-sheet with Ala6-Cys8 and with residues around Cys20. The HN protons of Ala6 and Cys8 exchange slowly into D_2O, as do those of Lys24 and Cys25. While the HN proton of Arg21 does not exchange slowly into D_2O, the resonance at 8.37 ppm might arise from the HN proton of Ser19. The former observation is rather surprising since, in a regular structure, the amide HN of Arg21 is expected to form a hydrogen bond across a β-turn (Arg21-Lys24) while the latter does not have an obvious hydrogen bonding partner since the sequence ends with the amide group on Cys25.

Within this small structural element, values of $^3J_{HN-H\alpha}$ are large (>8 Hz, characteristic of β-conformation) only for Ser19, Arg21, and Lys24 (Figure 1): those for Ala6, Lys7, and Cys25 are surprisingly small, while that for Cys20 is intermediate, indicating that the structure is rather irregular. Thus, while Ser19-Arg21 has a more regular β-conformation, the opposite strand, Ala6-Cys8, is more stable, as judged by

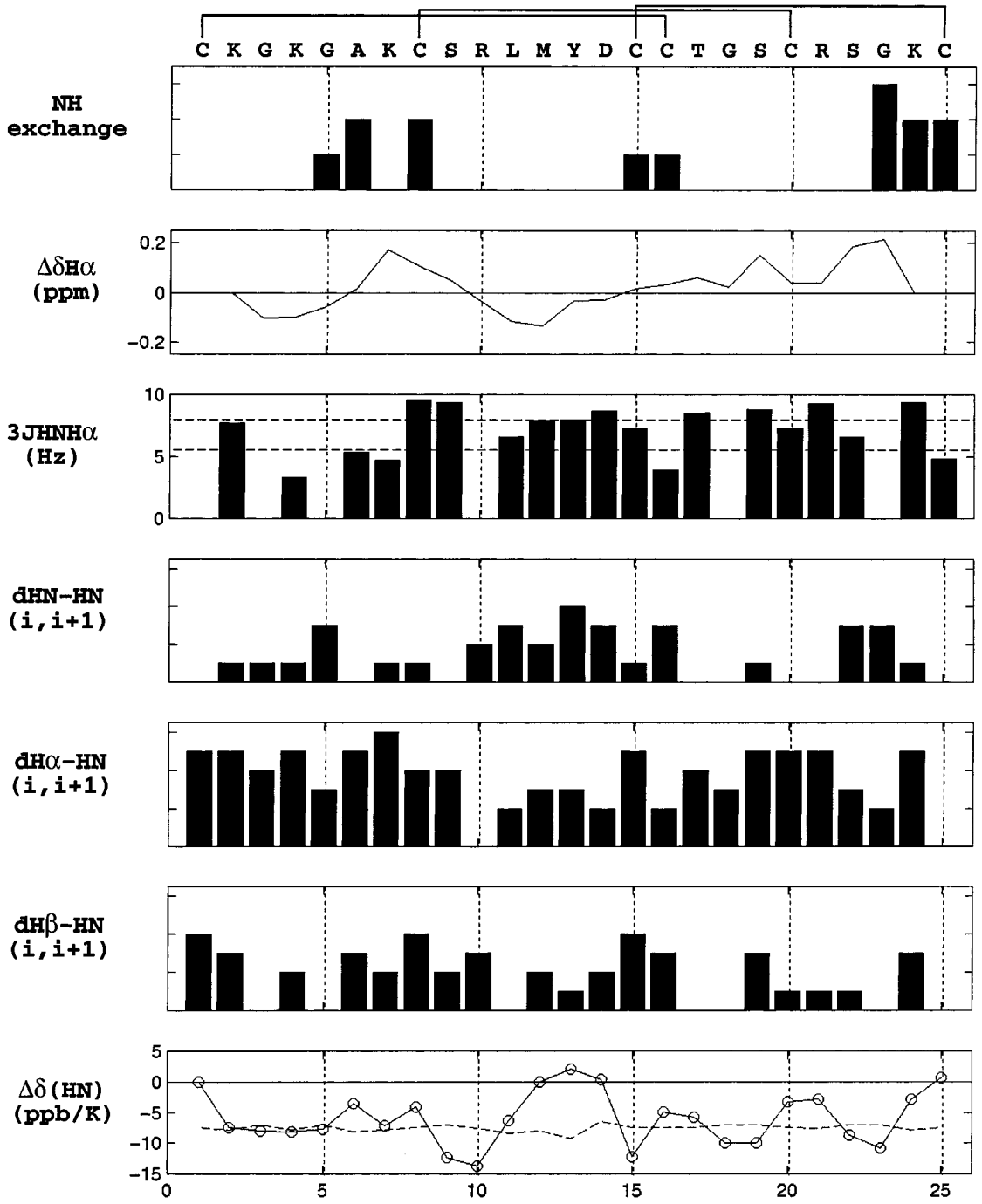

FIGURE 1: Summary of NMR data. The amino acid sequence is given along the top of the figure and sequence numbering along the bottom. The disulfide bridging pattern is shown above the amino acid sequence. NH exchange: taller bars indicate slower exchange into D_2O. $\Delta\delta$Hα: secondary chemical shifts of Hα resonances from "random coil" values. $^3J_{HNH\alpha}$: horizontal dashed lines are plotted at 5.5 and 8.0 Hz. d_{HN-HN}, $d_{H\alpha-HN}$, $d_{H\beta-HN}$: intensity of sequential NOEs. $\Delta\delta$(HN): rate of change in chemical shift of HN resonances with temperature.

the slow exchange of HN protons into D_2O. This structural element, involving Ala6-Cys8, Lys24-Cys25, and Ser19-Arg21, has been called a triple-stranded β-sheet (*8*,*9*,*11*) but is remarkably small and irregular, both in terms of structure and stability.

A $^3J_{HN-H\alpha}$ value close to 6.6 Hz, together with a strong $HN_i-H\alpha_i$ NOE, indicates a positive backbone ϕ angle. Only Ser22 could be clearly identified in this way, although positive ϕ angles could not be excluded for Leu11 and Tyr13.

Temperature Studies. Variation of the temperature between 275 and 304 K did not result in considerable changes in the patterns of NOEs detected in NOESY spectra, indicating that the integrity of the tertiary structure is maintained over this temperature range. However, a set of HN resonances, assigned to Arg10, Leu11, Met12, and Tyr13 were broadened considerably at low temperature. At higher temperatures, these resonances have line widths similar to those of other HN resonances. A set of aliphatic resonances, particularly those of Arg10, Met12, and Tyr13 were also broadened, as were the Cα−Hα cross-peaks of Arg10, Leu11, Met12, Asp14, and Cys15 in the ^{13}C-^1H HSQC spectrum (Figure 2). The localization of a group of broad resonances that

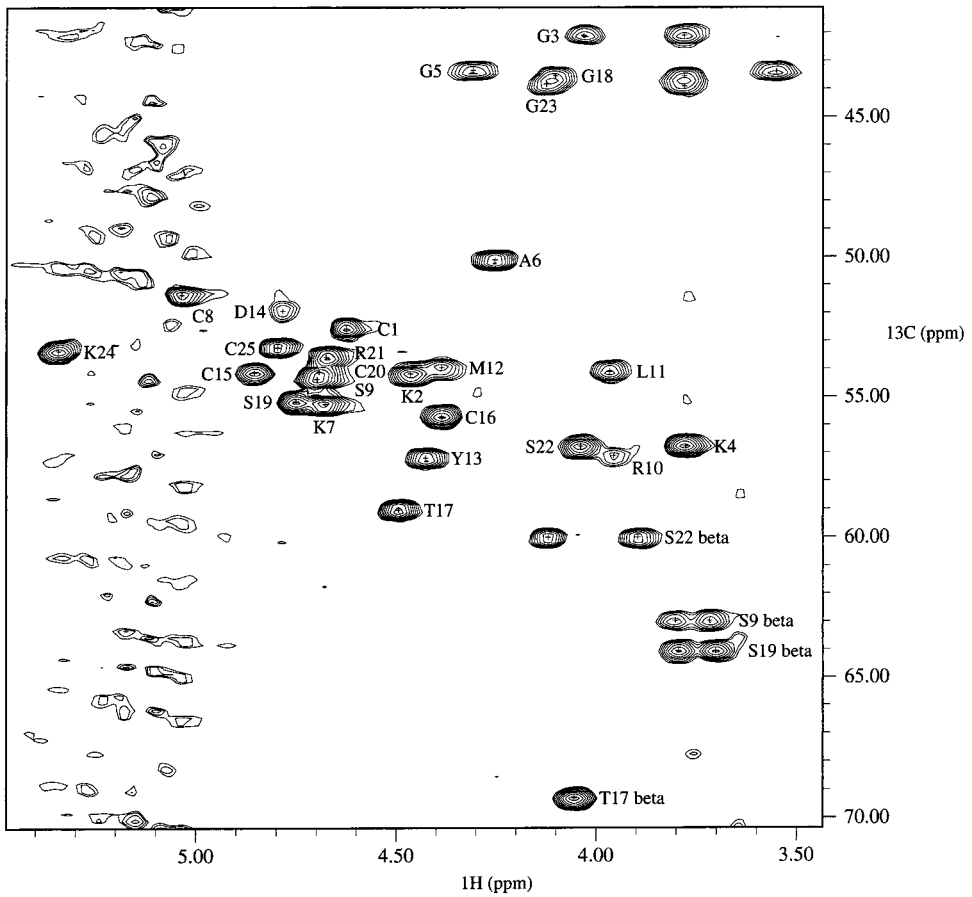

FIGURE 2: ^{13}C-^{1}H HSQC spectrum of ω-conotoxin MVIIA recorded at 600 MHz (^{1}H frequency), 283 K, and at natural abundance. Sample conditions were as described in Experimental Procedures. All $^{13}C\alpha^{1}-H\alpha$ and the $^{13}C_{\beta}{}^{1}-H\beta$ cross-peaks of serine and threonine residues are labeled.

sharpen with increased temperature suggests the presence of a conformational exchange on the millisecond time scale, just fast enough to average the chemical shift position in spectra recorded at the lowest temperature, but sufficiently slow for some broadening to be observed. The exchange rate must be slightly faster than the chemical shift differences between the exchanging species. As a rough estimate, the maximal difference in Hα chemical shifts of the exchanging species cannot reasonably exceed 1.5 ppm (*57*) or 750 Hz, giving a time scale for the exchange greater than 1.3 ms.

Temperature Coefficients. The temperature coefficients of HN resonances are related to temperature-dependent lengthening of average hydrogen bonding distances (*59*). Values that are smaller than "random coil" values are sometimes taken as an indication of involvement in hydrogen bonding and/or secondary structure (*59*). The temperature coefficients for residues Lys2-Cys8 (Figure 1) lie close to the values for the same residues in "random coil" peptides (*52*), with those of Ala6 and Cys8 dropping to lower values. This is consistent with Ala6-Cys8 forming a β-strand in which the HN proton of Lys7 is accessible to solvent while those of Ala6 and Cys8 are involved in hydrogen bonds. Indeed, the HN protons of Ala6 and Cys8 exchange slowly into D_2O (see above), and the Hα proton of Lys7 gives a $H\alpha_i-H\alpha_j$ NOE to Lys24.

The remaining two-thirds of the sequence exhibits highly anomalous behavior (Figure 1), possibly reflecting a loss of defined structure at higher temperature (*59*). While the low temperature coefficients for Cys16-Thr17 and Cys20-Arg21 might indicate hydrogen bonding or low solvent accessibility, those for Ser9, Arg10, Cys15, Gly18, Ser19, Ser22, and Gly23 are exceptionally high, rising to almost twice the values for the same residues in "random coil" peptides. In contrast, the temperature coefficients for Met12, Tyr13, Asp14, and Cys25 are not merely reduced (as observed for Ala6 and Cys8), but lie close to zero. Of these residues, both the HN proton of Gly23, in the first group, and that of Cys25, in the second, were observed to exchange slowly into D_2O, with the HN proton of Gly23 exchanging the most slowly of all. Similarly, the temperature coefficient for Ser19 is high while that for Arg21 is low: the HN proton of Ser19 may exchange slowly into D_2O, while that of Arg21 does not.

A number of aliphatic resonances also move considerably on raising the temperature. Those with the greatest changes in chemical shift between 275 and 304 K were Cys8 Hα and Hβ, Ser9 Hβ, Arg10 Hα, Leu11 Hα, Met12 Hα, Tyr13 Hα and Hβ, Asp14 Hβ, Cys15 Hβ, Cys20 Hβ, Arg21 Hα, and Cys25 Hβ.

A conformational exchange involving this sequence explains the observed broadening (^{13}C relaxation data confirm this, vide infra), and the effects of temperature on the chemical shifts of some resonances of aliphatic protons also reflect a conformational equilibrium. The affected residues include not only the central binding loop but also the residues of the flanking disulfide bridges (Cys8-Cys20 and Cys15-Cys25) and Arg21.

Relaxation Measurements and Spectral Density Values. To provide an indication of the quality of the relaxation data, measured at 600 MHz (^{1}H frequency) and natural abundance

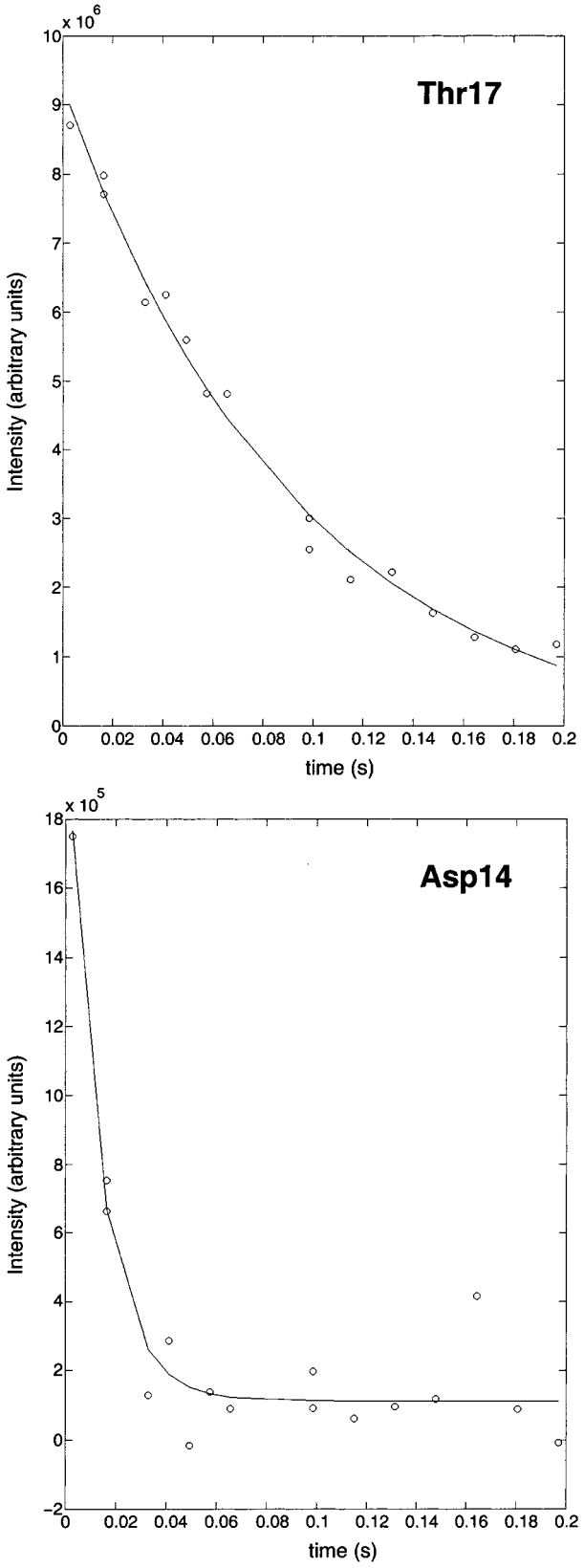

FIGURE 3: $R_C(C_{x,y})$ relaxation rates for two Cα nuclei in ω-conotoxin MVIIA, measured at 283 K and 600 MHz (^{1}H frequency). Experimental points are shown by open circles, and the best fit of a single exponential decay is represented by the solid line.

^{13}C, the raw $R_C(C_{x,y})$ data for the ^{13}Cα nuclei of two residues, Thr17 and Asp14, having small and large values, respectively, are shown in Figure 3. The cross-peak for Arg10 is weak and overlaps with the stronger cross-peak of Ser22, while those of Ser9 and Cys20, resolved at higher field strength, overlap partially.

Typically, a plot of $J(0)$ versus sequence reveals a flat baseline corresponding to the majority of residues, whose movement is largely that of overall tumbling of the molecule and a small degree of faster internal motion. The $J(0)$ values are expected to drop in the N- and C-termini and in flexible loops as the amplitude of faster motions increases. Here, residues in the N- and C-termini have $J(0)$ values close to those of the baseline, indicating that both termini are intimately involved in the tertiary structure (Figure 4). Increases in $J(0)$ from the baseline that are not accompanied by changes in values of the spectral density at other frequencies can arise only from exchange contributions (vide infra).

The errors on the values of $J(\omega_C)$ and $\langle J(\omega_H)\rangle$ are quite large (Figure 4), especially for the measurements made at 500 MHz (^{1}H frequency). This can be ascribed largely to the low sensitivity of measurements at natural abundance. The errors on $J(0)$ values are smaller, even for the residues affected by exchange contributions, where $R_C(C_{x,y})$ rates are fast. Values of the spectral density at ω_C calculated taking the form of the function around ω_H to be Lorentzian are systematically lower than those assuming the function to be flat, while the corresponding values at $\langle\omega_H\rangle$ are systematically higher. Only at $\langle\omega_H\rangle$ do the values exceed the error on the latter value.

The most striking feature of the plot of $J(0)$ versus sequence is the large increase in $J(0)$ for the segment Ser9-Cys15, indicating a significant contribution of exchange to $J(0)$. The residues most affected are Leu11 and Asp14, but the exchange contribution to $J(0)$, R_{ex}, depends on the *difference* in chemical shifts of the ^{13}C nuclei of the exchanging conformations ($\Delta\nu$):

$$R_{ex} = \frac{4\pi^2\Delta\nu^2 p_A p_B \tau_{ex}}{1 + \omega_1^2 \tau_{ex}^2} \qquad (8)$$

(where p_A and p_B are the populations of the states A and B, τ_{ex} is the exchange time, and ω_1 is the frequency of the spin-lock field), such that the term may be rendered null if $\Delta\nu = 0$; that is, if the chemical shifts of a particular nucleus in the exchanging states happen to be identical. Since $\Delta\nu$, p_A and p_B are unknown, τ_{ex} cannot be reliably estimated. Setting $p_A = p_B = 0.5$ and $\tau_{ex} = 2\pi/\Delta\nu$, the maximum possible value of R_{ex} can be estimated for values of $\Delta\nu$. This suggests a maximum value of τ_{ex} of around 4 ms.

After manual filtering of spectral density values affected by exchange, a fit to the plot of $J(\omega_C)$ versus $J(0)$ at 600 MHz (*36*) indicates a correlation time for overall tumbling of the molecule of 3.8 ns, while internal motion is characterized by a correlation time of 240 ps. The error on the determination of $J(\omega_C)$ makes the estimate of the correlation time for overall tumbling rather imprecise: taking instead the baseline values of $J(0)$ at 500 and 600 MHz (^{1}H frequency) and assuming an order parameter of 0.8 for these residues gives correlation times for overall tumbling of 2.8 and 2.7 ns. These values are rather large for a molecule of the size of ω-conotoxin MVIIA but are sensitive to the setting of the baseline and assume no exchange contributions to these points.

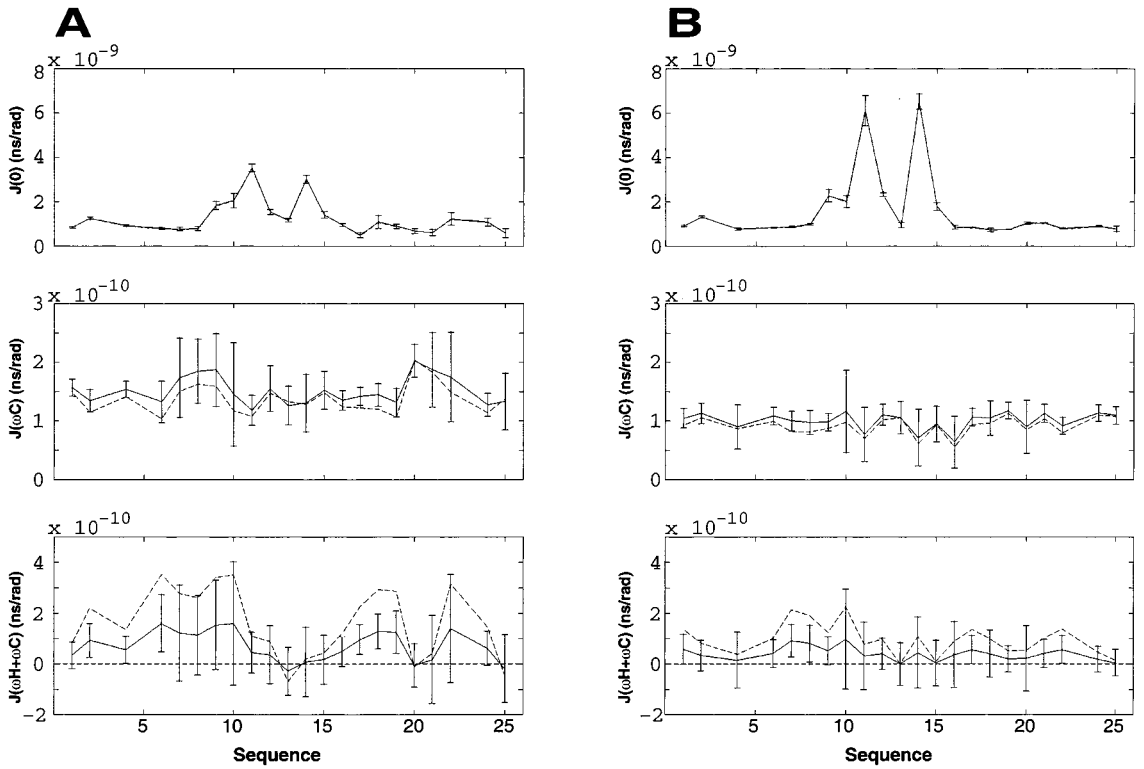

FIGURE 4: Values of the spectral density function, $J(\omega)$, determined for the $^{13}C\alpha$ nuclei of ω-conotoxin MVIIA at 283 K and at (A) 500 MHz and (B) 600 MHz (^1H frequency). The solid line connects points calculated using the reduced spectral density mapping approach, assuming $J(\omega)$ to be flat at high frequency. The dashed line connects points calculated using a Lorentzian fit to the high-frequency data. Data for Thr 17 are reported at sequence numbers 17 (Thr17 $^{13}C\alpha$) and 18 (Thr17 $^{13}C\beta$).

Diffusion Measurements. The value of the translational diffusion constant for ω-conotoxin MVIIA in H_2O at 293 K is 2.0×10^{-10} m^2 s$^{-1} \pm 0.05$. Extrapolation from values for lysozyme (used as a model monomeric protein for which the diffusion coefficient has been determined by several techniques (*60,61*)) to the molecular mass of ω-conotoxin MVIIA, assuming both molecules to be spherical, gives a value of 1.8×10^{-10} m^2 s^{-1}. This small difference may be due to the slightly flattened shape of the conotoxin (the axial ratio is 1.4). The value indicates that ω-conotoxin MVIIA is monomeric in solution under these conditions and may be translated into a rotational correlation time of 2.2 ns in D_2O at 283 K. This value is in good agreement with that estimated from the longest axis of ω-conotoxin MVIIA (approximately 11.4 Å) using the Stokes−Einstein relation and allowing for solvation ($\tau_c = 2.24$ ns).

Tertiary Structure. ω-Conotoxin MVIIA adopts a compact fold defined by a small, irregular triple-stranded β-sheet and three disulfide bridges. Hydrogen bonds and dihedral angle restraints introduced during the calculations are given in Supporting Information. The effects of conformational exchange on the calculated structures must, however, be considered.

Calculations without χ_3 Constraints. The results of calculations performed using standard protocols with no constraints on the χ_3 angles of the three disulfide bridges appear, at first, to be reasonable (Table 1, Figure 5). While portions of the structure are better defined (average pairwise rmsd values, calculated over a five-residue window, <0.35 Å), the local structure is less well-defined for residues in the binding loop (Ser9 to Tyr13) and those following Cys16 (Cys16 to Ser19). The average pairwise rmsd. calculated over all backbone atoms is 0.67 Å, dropping to 0.55 Å when these portions are excluded from the fit. The triple-stranded β-sheet is indeed highly irregular, and the sequence between Lys4 and Cys8 adopts two well-defined conformations (Figure 6), with neither being associated with a lower energy than the other. The set of structures suffers, however, from very poor geometry for the disulfide bridges (Figure 5). The structures otherwise have very good covalent geometry and satisfy well the experimental data, but the set of NOEs, coupling constants, and hydrogen bonds results in distorted bridges.

Residues of the central binding loop of ω-conotoxin MVIIA are affected by conformational exchange on the millisecond time scale, fast enough to average chemical shifts. The effects of this exchange on the data used to calculate structures must be considered: both the intensity

Table 1. Energy Terms of Final Sets of Structures of ω-Conotoxin MVIIA[a]

	no χ_3	χ_3 positive	χ_3 negative
E_{tot}	27.97 (2.86)	51.93 (4.52)	50.95 (3.92)
E_{bonds}	2.10 (0.30)	4.29 (0.51)	3.50 (0.40)
E_{angles}	8.46 (1.00)	16.84 (1.95)	16.06 (2.16)
E_{impr}	2.91 (1.35)	3.39 (1.56)	2.40 (0.49)
E_{vdW}	3.29 (0.81)	6.71 (1.55)	5.20 (0.96)
E_{NOE}	10.81 (1.63)	19.38 (2.07)	23.35 (2.04)
E_{dihe}	0.41 (0.39)	1.32 (0.62)	0.44 (0.47)
pairwise rmsd (Å)[b]	0.55 (0.19)	0.53 (0.15)	0.46 (0.13)

[a] The average energies are reported in kcal mol^{-1}; standard deviation is given in parentheses. Statistics for structures calculated with no χ_3 constraints and for those with positive χ_3 for Cys8-Cys20 are from sets of 25 structures; those with negative χ_3 for Cys8-Cys20 are from a set of seven structures selected using the same E_{tot} cut-off as for the set with positive χ_3. [b] Pairwise root mean square deviation calculated over the backbone atoms of residues Cys1-Cys8 and Cys20-Cys25.

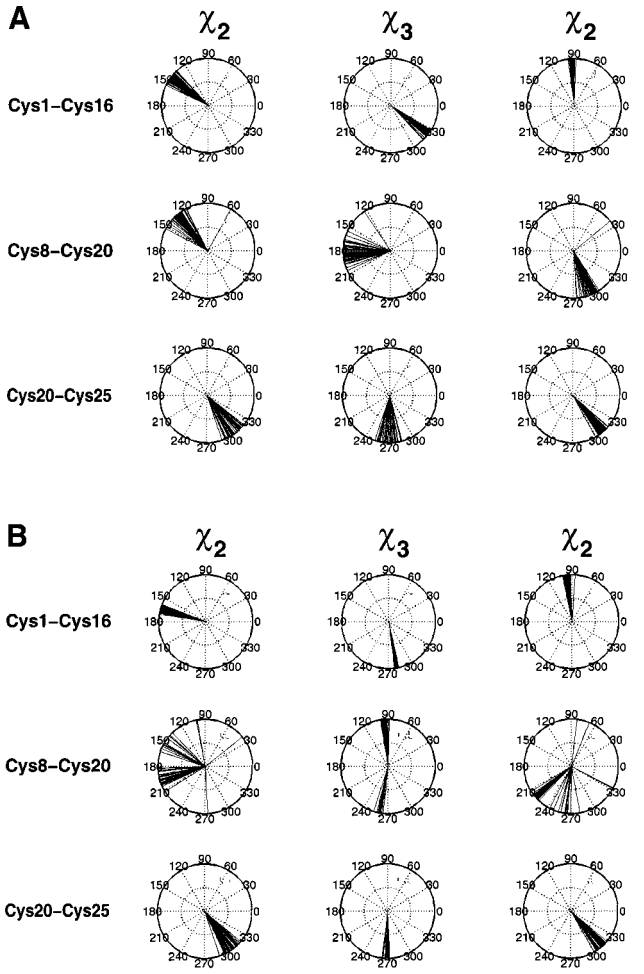

FIGURE 5: Values of the χ_2 and χ_3 dihedral angles across the three disulfide bridges of ω-conotoxin MVIIA in 50 structures calculated (A) without and (B) with constraints on the χ_3 dihedral angles.

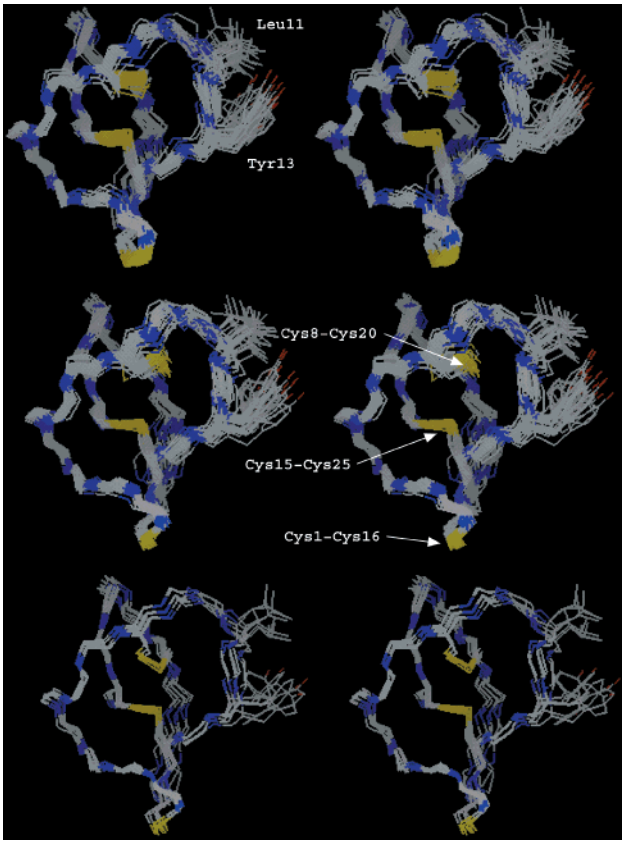

FIGURE 6: Families of structures of ω-conotoxin MVIIA. For each, the backbone is shown with the side chains of the six cysteine residues, Leu11 and Tyr13. Atoms are colored according to type. The upper panel shows 25 structures calculated with no constraints on the geometry of the disulfide bridges. The lower panels show structures calculated with constraints on the χ_3 angles of the disulfide bridges, separated into two sets: 25 structures (middle panel) with the Cys8-Cys20 $\chi_3 \approx +90°$ and seven structures with $\chi_3 \approx -90°$.

of observed NOEs and the values of coupling constants will be averaged. The r^{-6} dependence of the intensity of the NOE on the distance between nuclei causes shorter distances to dominate the observed intensity. The list of distance constraints will therefore be biased toward the shorter distances from each of the two (or more) exchanging conformers. Here, the set of distances can be satisfied but at the expense of the disulfide bridge conformations.

Calculations with χ_3 Constraints. Imposition of dihedral angle constraints on the χ_3 angle across the disulfide bridges forces the geometry of the bridges to be close to ideal (Figure 5). A penalty is paid in satisfying other experimental constraints, causing higher total energies for calculated structures (Table 1). Analysis of the disulfide bridge conformations allows the 50 lowest energy structures to be divided into two families, differing in the conformation of the disulfide bridge Cys8-Cys20. The families contain 36 and 14 members with χ_3 values around $+90°$ and $-90°$, respectively. The average pairwise rmsd calculated over all backbone atoms of the first set remains 0.67 Å (dropping to 0.53 Å when less well-defined portions are excluded from the fit), while for the second set the values are 0.55 and 0.46 Å.

The division into families caused by imposition of constraints on χ_3 suggests a possible origin for the conformational exchange occurring in ω-conotoxin MVIIA in solution. Disulfide bridge isomerization of Cys8-Cys20 may be occurring at a rate that averages the chemical shifts in the two conformations, but broadens a set of resonances at low temperature and contributes to $J(0)$ (Figure 7).

Chemical Shift Calculations. Semiempirical calculations of proton chemical shifts were performed for the 50 lowest energy structures of ω-conotoxin MVIIA following X-PLOR refinement with χ_3 angles constrained. The set of structures contains two families that differ in the conformation of the Cys8-Cys20 disulfide bridge. Calculated chemical shifts were averaged over the whole set and over the two families of structures separately, but the results were not statistically different. For the whole set, the overall average difference between calculated and observed chemical shifts is 0.04 ppm with a root-mean-square deviation of 0.24 ppm. Individual structures have a significantly larger rms difference between calculated and experimental chemical shifts (0.41 to 0.59 ppm), compared to the difference of 0.24 ppm obtained by averaging over the 50 structures. These values are consistent with the error range reported for good quality NMR structures (*62*).

Several residues have Hα chemical shifts that differ from the "random coil" values by more than 0.3 ppm: Lys4, Gly5, Lys7, Cys8, Arg10, Leu11, Cys15, Arg21, Ser22, Lys24. The conformational shifts calculated for the Hα nuclei explain the observed chemical shifts in many instances. For

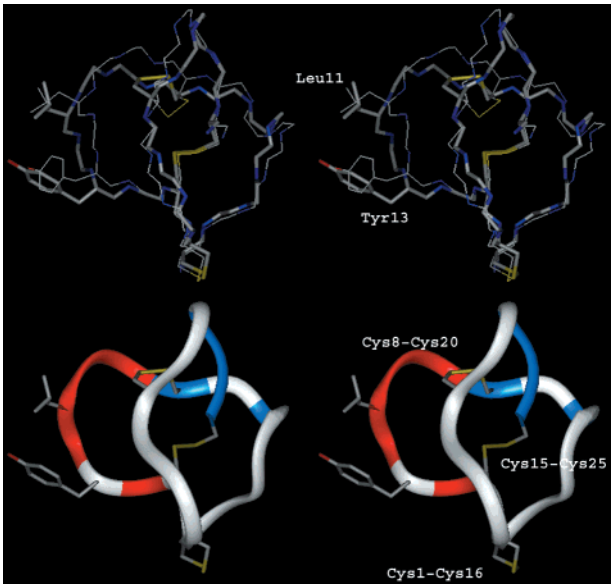

FIGURE 7: Lowest energy structures of ω-conotoxin MVIIA calculated with constraints on the χ_3 dihedral angle across disulfide bridges. The side chains of the six cysteine residues, Leu11, and Tyr13 are shown. Upper panel: structure with Cys8-Cys20 $\chi_3 \approx +90°$ is represented by thick sticks while the structure with Cys8-Cys20 $\chi_3 \approx -90°$ is in thin lines. Lower panel: residues with slowly exchanging backbone amide protons are mapped onto the ribbon in light blue: residues affected by exchange contributions to $J(0)$ are mapped onto the ribbon in red.

example, the upfield shift of Leu11 is due to the ring current of Tyr13. Peptide bond magnetic anisotropy and electrostatic contributions vary with ϕ and ψ angles. These form the basis of the negative structural chemical shifts for α-helices and positive chemical shifts for β-sheets, used in the chemical shift index (*53*,*57*). This effect explains the chemical shifts observed for Lys4, Arg21, and Ser22 as well as a large number of the smaller structural shifts of Hα protons.

In several cases, the predicted Hα chemical shifts are in poor agreement with the observed values, such as Cys1, Lys2, Gly3, Gly5, Lys7, Cys8, Arg10, Cys15, Cys20, Lys24, and Cys25. This set includes all but one cysteine residue and other Hα protons, such as Lys24, that are close in space to the disulfide bridges. On average, disulfide bridges have a deshielding effect on neighboring atoms (F. Sirockin, manuscript in preparation). This contribution is not taken into account in the current model and seems to fit the noted discrepancies, i.e., calculated Cys Hα shifts are too shielded compared to the experimental values. For Lys2, Gly3, Gly5, Lys7, and Arg10, the discrepancy between calculated and observed chemical shifts could be due to solvation as these residues are mostly exposed.

Calculated chemical shifts for other carbon-attached protons are generally in satisfactory agreement with observed values: discrepancies occur for the same residues as for Hα chemical shifts, such as Lys24 and Cys25.

Motional averaging, as is observed for residues Arg10-Tyr13, may also lead to discrepancies between calculated and observed chemical shifts (*63*). In particular, the region undergoing motion contains the only aromatic residue in ω-conotoxin MVIIA, Tyr13. The side chain of Tyr13 is directed toward to the solvent in calculated structures, such that the ring current contribution to the chemical shift dispersion is small and affects only few residues. The absolute value of the calculated ring current contribution is larger than 0.1 ppm only for Leu11 and Met12 (the effect on Tyr13 itself being included in the "random coil" contribution). Thus, in this particular case, the discrepancy between calculated and observed chemical shifts is not significantly worse for the loop residues, with the exception of Arg10 (see above), since they are largely exposed to solvent and have chemical shifts that either are close to "random coil" values or are directly influenced by Tyr13.

DISCUSSION

The structure of ω-conotoxin MVIIA in solution is a compact fold, defined principally by a set of three disulfide bridge and a tiny triple-stranded β-sheet that is irregular both in terms of its structure and its stability. In most respects, the calculated structure resembles closely those determined previously by other groups (*8*,*9*,*11*), although the set of structures from the most detailed study (*11*) represents a unique conformation. The authors worked at both 283 and 293 K, so similar results would be expected. Fewer backbone amide protons were observed to exchange into D_2O in this study, and fewer backbone ϕ angles could be confidently constrained. Nonetheless, the structure is largely well-defined with residues Ser9-Tyr13 and Cys16-Ser19 being less well-defined by constraints derived from NMR measurements. The former segment contains residues critical for binding to N-type calcium channels.

Relaxation measurements do not confirm increased amplitudes of fast internal motions for the binding loop. Rather, they reflect a rather tight fold for the molecule that behaves essentially as a rigid unit tumbling in solution with a uniform degree of faster internal motions. The spectral density values for the residues in the loop are, however, greatly perturbed by contributions from slow conformational exchange processes. Several other lines of evidence show that the molecule is undergoing conformational exchange between two or more states on the millisecond time scale. Broad resonances and the temperature dependence of the resonances of some aliphatic protons all reflect this exchange. Furthermore, the data localize the exchange to the peptide sequence between Cys8 and Cys15, the loop containing a number of residues required for receptor binding.

The presence of conformational exchange causes problems in the interpretation of other NMR data. In particular, the detected nuclear Overhauser effects either result from all species present or are time-averaged, depending on the characteristic time for the conformational exchange. Since these effects are used to derive distance constraints for input into calculation of the tertiary structure of the molecule, but do not arise from a single structure or rapid fluctuations about a single structure, the results of such calculations are inevitably flawed. This was particularly clear here in the poor geometry of the disulfide bridges.

Isomerization of the conformation of disulfide bridge Cys8-Cys20 appears to be central to the conformational exchange. If conditions could be found in which the exchanging species could be independently observed, the hypothesis could be investigated further, but to date, attempts to work at lower temperature, in aqueous solution, or in cryoprotective mixtures have not succeeded. In recent studies of

BPTI (*64*), the rates of conformational exchange for a set of residues were increased more than 2-fold on removal of the disulfide bridge Cys14-Cys38. The authors suggest that the disulfide bridge is not responsible for the exchange but may help accommodate the motions. It may be rather that isomerization of the disulfide bridge serves to control the rate of the exchange process. This control may or may not have functional significance. For ω-conotoxin MVIIA, in which it is the key binding loop that is undergoing conformational exchange, the rate may well be expected to effect activity, although this remains to be demonstrated experimentally.

The conformational exchange may require the differing stabilities of the β-strands to occur at a certain rate at relevant temperatures. A more regular and stable structure might disfavor the conformational exchange and suggests that its presence is by design rather than being accidental, possibly allowing the molecule to bind to two different receptor subtypes in its prey. Whether such processes are common to other ω-conotoxins or are particular to ω-conotoxin MVIIA remains to be seen. No evidence for conformational exchange has been reported for ω-conotoxins GVIA (*5*−*7*) and MVIIC (*10*). The deposited structures of the latter, however, contain significant distortions of backbone ω dihedral angles, suggesting that experimental data from two exchanging conformers may have been satisfied at the expense of covalent geometry. The spectra of ω-conotoxin MVIID reveal a small population of a second conformation (*65*) but no exchange between the major and minor conformers was detected.

α-Conotoxins also reveal differing behavior. While α-conotoxins ImI (*66*−*68*) and MII (*69*) exist as a single conformer in solution with no evidence of conformational exchange, α-conotoxin MI shows multiple conformers in slow exchange, apparently related to *cis*- and *trans*-conformations of Pro6 (*70,71*). α-Conotoxin GI, on the other hand, has two distinct conformations in solution that are in fast exchange (*72*). While the pattern of disulfide bridges in all four molecules is identical, the number of residues separating the cysteines differs, offering a straightforward explanation for part of the observations. The differences between α-conotoxins MI and GI, however, must relate to specific differences in the amino acid side chains. Such considerations are clearly of importance for other classes of biologically active molecules (see, for example, ref *73*).

The compact, triple-stranded β-structure of ω-conotoxin MVIIA presents to the receptor a set of functional groups that defines its affinity and specificity. The structure cannot, however, be viewed simply as a rigid scaffold supporting a function defined by the nature of the side chains and cannot, therefore, be considered either as a scaffold onto which an alternative function may be grafted. This appears to be equally true of some α-conotoxins. The studies presented here show that the framework has a number of characteristics that bear on its function and emphasize the importance of the dynamic characterization of molecules of biological interest.

In light of these observations, the suggestion that the structures of molecules such as conotoxins may be useful for ligand design requires careful consideration. In designing ligands, is a more or less rigid scaffold required? Is the exchange process of use or should it be eliminated from a designed molecule? If the latter, which of the exchanging conformations should be used as a template?

More generally, ligands to a particular receptor may often be inherently mobile, adopting a more defined, or single, structure only on binding to the receptor. This loss of flexibility on binding imposes an entropic penalty on the interaction that must be overcome by enthalpic terms or other factors, such as the gain of entropy associated with the displacement of ordered solvent molecules. In such a case, structural studies of a flexible ligand in solution or in crystalline form may assist only little in understanding its interactions with a receptor and guiding subsequent drug design efforts. Characterization of the nature and the time scales of internal motions may assist, however, in understanding the mechanisms of action of such ligands.

ACKNOWLEDGMENT

The authors thank Claude Ling (ESBS, Strasbourg) for invaluable technical assistance and Drs. T. E. Howe and Will Prowse (Eli Lilly) for their interest and support.

SUPPORTING INFORMATION AVAILABLE

^{1}H and ^{13}C resonance assignments and the hydrogen bonds and dihedral angles included as restraints in structure calculations.

REFERENCES

1. Olivera, B. M., Rivier, J., Clark, C., Ramilo, C. A., Corpuz, G. P., Abogadie, F. C., Mena, E. E., Woodward, S. R., Hillyard, D. R., and Cruz, L. J. (1990) *Science 249*, 257−263.
2. Olivera, B. M., Cruz, L. J., de Santos, V., LeCheminant, G. W., Griffin, D., Zeikus, R., McIntosh, J. M., Galyean, R., Varga, J., Gray, W. R., and Rivier, J. (1987) *Biochemistry 26*, 2086−2090.
3. Olivera, B. M., Miljanich, G. P., Ramachandran, J., and Adams, M. E. (1994) *Annu. Rev. Biochem. 63*, 823−867.
4. Myers, R. A., Cruz, L. J., Rivier, J. E., and Olivera, B. M. (1993) *Chem. Rev. 93*, 1923−1936.
5. Pallaghy, P. K., Duggan, B. M., Pennington, M. W., and Norton, R. S. (1993) *J. Mol. Biol. 234*, 405−420.
6. Sevilla, P., Bruix, M., Santoro, J., Gago, F., García, A. G., and Rico, M. (1993) *Biochem. Biophys. Res. Commun. 192*, 1238−1244.
7. Skalicky, J. J., Metzler, W. J., Ciesla, D. J., Galdes, A., and Pardi, A. (1993) *Protein Sci. 2*, 1591−1603.
8. Basus, V. J., Nadasdi, L., Ramachandran, J., and Miljanich, G. P. (1995) *FEBS Lett. 370*, 163−169.
9. Kohno, T., Kim, J. I., Kobayashi, K., Kodera, Y., Maeda, T., and Sato, K. (1995) *Biochemistry 34*, 10256−10265.
10. Farr-Jones, S., Miljanich, G. P., Nadasdi, L., Ramachandran, J., and Basus, V. J. (1995) *J. Mol. Biol. 248*, 106−124.
11. Nielsen, K. J., Thomas, L., Lewis, R. J., Alewood, P. F., and Craik, D. J. (1996) *J. Mol. Biol. 263*, 297−310.
12. Pallaghy, P. K., Nielsen, K. J., Craik, D. J., and Norton, R. S. (1994) *Protein Sci. 3*, 1833−1839.
13. Lampe, R. A., Lo, M. M. S., Keith, R. A., Horn, M. B., McLane, M. W., Herman, J. L., and Spreen, R. C. (1993) *Biochemistry 32*, 3255−3260.
14. Sato, K., Park, N.-G., Kohno, T., Maeda, T., Kim, J. I., Kato, R., and Takahashi, M. (1993) *Biochem. Biophys. Res. Commun. 194*, 1292−1296.
15. Nadasdi, L., Yamashiro, D., Chung, D., Tarczy-Hornoch, K., Adriaenssens, P., and Ramachandran, J. (1995) *Biochemistry 34*, 8076−8081.
16. Kim, J. I., Takahashi, M., Ogura, A., Kohno, T., Kudo, Y., and Sato, K. (1994) *J. Biol. Chem. 269*, 23876−23878.

17. Kim, J. I., Takahashi, M., Ohtake, A., Wakamiya, A., and Sato, K. (1995) *Biochem. Biophys. Res. Commun. 206*, 449−454.
18. Kim, J. I., Takahashi, M., Martin-Moutot, N., Seagar, M. J., Ohtake, A., and Sato, K. (1995) *Biochem. Biophys. Res. Commun. 214*, 305−309.
19. States, D. J., Haberkorn, R. A., and Ruben, D. J. (1982) *J. Magn. Reson. 48*, 286−292.
20. Marion, D., and Wüthrich, K. (1983) *Biochem. Biophys. Res. Commun. 113*, 967−974.
21. Aue, W. P., Bartholdi, E., and Ernst, R. R. (1976) *J. Chem. Phys. 64*, 2229−2246.
22. Braunschweiler, L., and Ernst, R. R. (1983) *J. Magn. Reson. 53*, 521−528.
23. Bax, A., and Davis, D. G. (1985) *J. Magn. Reson. 65*, 355−360.
24. Jeener, J., Meier, B. H., Bachmann, P., and Ernst, R. R. (1979) *J. Chem. Phys. 71*, 4546−4553.
25. Piotto, M., Saudek, V., and Sklenář, V. (1992) *J. Biomol. NMR 2*, 661−665.
26. Sklenář, V., Piotto, M., Leppik, R., and Saudek, V. (1993) *J. Magn. Reson. Series A 102*, 241−245.
27. Bodenhausen, G., and Ruben, D. J. (1980) *Chem. Phys. Lett. 69*, 185−189.
28. Cavanagh, J., Palmer, A. G., III, Wright, P. E., and Rance, M. (1991) *J. Magn. Reson. 91*, 429−436.
29. Shaka, A. J., Barker, P. B., and Freeman, R. (1985) *J. Magn. Reson. 64*, 547−552.
30. Dayie, K. T., and Wagner, G. (1994) *J. Magn. Reson. Series A 111*, 121−126.
31. Peng, J. W., and Wagner, G. (1992) *J. Magn. Reson. 98*, 308−332.
32. Peng, J. W., and Wagner, G. (1992) *Biochemistry 31*, 8571−8586.
33. Farrow, N. A., Zhang, O., Szabo, A., Torchia, D. A., and Kay, L. E. (1995) *J. Biomol. NMR 6*, 153−162.
34. Ishima, R., and Nagayama, K. (1995) *J. Magn. Reson. Series B 108*, 73−76.
35. Peng, J. W., and Wagner, G. (1995) *Biochemistry 34*, 16733−16752.
36. Lefèvre, J.-F., Dayie, K. T., Peng, J. W., and Wagner, G. (1996) *Biochemistry 35*, 2674−2686.
37. Ye, C., Fu, R., Hu, J., Hou, L., and Ding, S. (1993) *Magn. Reson. Chem. 31*, 699−704.
38. Atkinson, R. A., and Lefèvre, J.-F. (1999) *J. Biomol. NMR 13*, 83−88.
39. Kirkpatrick, S., Gelatt, C. D., Jr., and Vecchi, M. P. (1983) *Science 220*, 671−680.
40. Goffe, W. L., Ferrier, G. D., and Rogers, J. (1994) *J. Econometrics 60*, 65−99.
41. Martin, J. F., Selwyn, L. S., Vold, R. R., and Vold, R. L. (1982) *J. Chem. Phys. 76*, 2632−2634.
42. Zax, D. B., and Pines, A. (1983) *J. Chem. Phys. 78*, 6333−6334.
43. Kay, L. E., and Prestegard, J. H. (1986) *J. Magn. Reson. 67*, 103−113.
44. Stejskal, E. O., and Tanner, J. E. (1965) *J. Chem. Phys. 42*, 288−292.
45. Wüthrich, K., Billeter, M., and Braun, W. (1983) *J. Mol. Biol. 180*, 949−961.
46. Karplus, M. (1959) *J. Chem. Phys. 30*, 11−15.
47. Pardi, A., Billeter, M., and Wüthrich, K. (1984) *J. Mol. Biol. 180*, 741−751.
48. Ludvigsen, S., and Poulsen, F. M. (1992) *J. Biomol. NMR 2*, 227−233.
49. Wagner, G., Braun, W., Havel, T. F., Schaumann, T., Gō, N., and Wüthrich, K. (1987) *J. Mol. Biol. 196*, 611−639.
50. Brünger, A. (1992) *X-PLOR Software Manual, version 3.1*, Yale University Press, New Haven, CT.
51. Ösapay, K., and Case, D. A. (1991) *J. Am. Chem. Soc. 113*, 9436−9444.
52. Merutka, G., Dyson, H. J., and Wright, P. E. (1995) *J. Biomol. NMR 5*, 14−24.
53. Ösapay, K., and Case, D. A. (1994) *J. Biomol. NMR 4*, 215−230.
54. Sitkoff, D., and Case, D. A. (1997) *J. Am. Chem. Soc. 119*, 12262−12273.
55. Wüthrich, K. (1986) *NMR of Proteins and Nucleic Acids*, J. Wiley, New York, .
56. Pastore, A., and Saudek, V. (1990) *J. Magn. Reson. 90*, 165−176.
57. Wishart, D. S., Sykes, B. D., and Richards, F. M. (1991) *J. Mol. Biol. 222*, 311−333.
58. Wishart, D. S., Sykes, B. D., and Richards, F. M. (1992) *Biochemistry 31*, 1647−1651.
59. Baxter, N. J., and Williamson, M. P. (1997) *J. Biomol. NMR 9*, 359−369.
60. Dubin, S. B., Clarck, N. A., and Benedeck, G. B. (1971) *J. Chem. Phys. 54*, 5158−5164.
61. Altieri, A. S., Hinton, D. P., and Byrd, R. A. (1995) *J. Am. Chem. Soc. 117*, 7566−7567.
62. Williamson, M. P., Kikuchi, J., and Asakura, T. (1995) *J. Mol. Biol. 247*, 541−546.
63. Mer, G., Dejaegere, A., Stote, R., Kieffer, B., and Lefèvre, J.-F. (1996) *J. Chem. Phys. 100*, 2667−2674.
64. Beeser, S. A., Oas, T. G., and Goldenberg, D. P. (1998) *J. Mol. Biol. 284*, 1581−1596.
65. Civera, C., Vásquez, A., Sevilla, J. M., Bruix, M., Gago, F., García, A. G., and Sevilla, P. (1999) *Biochem. Biophys. Res. Commun. 254*, 32−35.
66. Gouda, H., and Hirono, S. (1999) *Biochim. Biophys. Acta 1431*, 384−394.
67. Maslennikov, I. V., Shenkarev, Z. O., Zhmak, M. N., Ivanov, V. T., Methfessel, C., Tsetlin, V. I., and Arseniev, A. S. (1999) *FEBS Lett. 444*, 275−280.
68. Rogers, J. P., Luginbühl, P., Shen, G. S., McCabe, R. T., Stevens, R. C., and Wemmer, D. E. (1999) *Biochemistry 38*, 3874−3882.
69. Hill, J. M., Oomen, C. J., Miranda, L. P., Bingham, J.-P., Alewood, P. F., and Craik, D. J. (1998) *Biochemistry 37*, 15621−15630.
70. Gray, W. R., Rivier, J. E., Galyean, R., Cruz, L. J., and Olivera, B. M. (1983) *J. Biol. Chem. 258*, 12247−12251.
71. Gouda, H., Yamazaki, K., Hasegawa, J., Kobayashi, Y., Nishiuchi, Y., Sakakibara, S., and Hirono, S. (1997) *Biochim. Biophys. Acta 1343*, 327−334.
72. Maslennikov, I. V., Sobol, A. G., Gladky, K. V., Lugovskoy, A. A., Ostrovsky, A. G., Tsetlin, V. I., Ivanov, V. T., and Arseniev, A. S. (1998) *Eur. J. Biochem. 254*, 238−247.
73. Wikström, A., Berglund, H., Hanbraeus, C., van der Berg, S., and Härd, T. (1999) *J. Mol. Biol. 289*, 963−979.

BI992651H